PAPER

Vacuum thermally evaporated polymeric zinc acrylate as an organic interlayer of organic/inorganic multilayer passivation for flexible organic thin-film transistors

Won Min Yun,[a] **Jaeyoung Jang,**[a] **Sooji Nam,**[a] **Yong Jin Jeong,**[a] **Lae Ho Kim,**[a] **Seyeol Park,**[a] **Sang Joon Seo**[*b] **and Chan Eon Park**[*a]

Polymeric zinc acrylate (pZA) was introduced as an organic interlayer for the inorganic/organic multilayer passivation of flexible organic thin film transistors (OTFTs). The pZA film was deposited by thermally evaporating a zinc diacrylate (ZDA) monomer under high vacuum ($<10^{-5}$ Torr) and applying UV irradiation. The conversion of ZDA into a polymeric phase was confirmed by FTIR analysis, breakdown voltage measurements and the photopatternability of the film before and after UV irradiation. Vacuum-thermally evaporated pZA film showed good surface smoothness and a high permeation activation energy (53 kJ mol^{-1}) compared to conventional polymeric films. As an interlayer for multilayer passivation, vacuum-thermally evaporated silicon monoxide (SiO) was introduced as the inorganic counterpart of the pZA interlayer. A multilayer film comprising 6.5 pairs of layers showed a water vapor transmission rate (WVTR) of 0.055 g m^{-2} per day, a 25-fold improvement over the WVTR of a single SiO film (1.207 g m^{-2} per day). OTFTs encapsulated with 6.5 pairs of polymeric zinc acrylate/silicon monoxide layers showed prolonged stability over 97 days. In addition, the passivation layer did not show crack formation, and sustained barrier characteristics, even after 500 bending tests.

1. Introduction

Organic electronic devices on plastic substrates have attracted considerable attention for their potential advantageous properties, including flexibility, simplicity of mass production and low cost. Therefore, extensive studies have been performed with the goal of commercializing organic electronic devices (OPVs, OTFTs and OLEDs). The results of such studies are applicable across several types of organic electronic device, such as OLEDs.[1] The intrinsic vulnerabilities of organic electronic devices in the presence of moisture and oxygen under ambient air conditions require the fabrication of an effective permeation barrier that can prevent the penetration of water vapor or oxygen into the organic electronic devices. Permeation barriers are critical for securing product reliability in the organic electronics market.[2-6] For this reason, devices are commonly sealed with a glass or metal lid to preserve the device performance. However, the rigid characteristics of glass or metal lids complicate the

passivation of large-area or flexible organic electronic devices, two qualities that are unique to organic electronics.

A thin film barrier coating method, in which a barrier film is directly deposited onto the devices, was introduced as an alternative approach to the passivation of organic electronic devices.[7] Plasma enhanced chemical vapor deposition (PECVD),[8] plasma enhanced atomic layer deposition (PEALD),[9-11] sputtering,[12] thermal evaporation, inkjet printing[13] and spin coating processes[14,15] were tested in an effort to deposit a thin barrier film onto the organic electronic device. Among those efforts, organic/inorganic multilayer structures have been frequently used as effective passivation methods that satisfy the most stringent performance requirements of OLEDs [water vapor transmission rate (WVTR) < 10^{-6} g m^{-2} per day].[16-18] In multilayer systems, barrier films are composed of alternate stacks of organic and inorganic layers. Inorganic layers, generally consisting of metallic oxide or nitride compounds, play a role as the main barrier film. However, an inorganic single layer is prone to the formation of pinholes and cracks in the film, which are known to the main permeation path for water vapor. As a result, a single inorganic layer shows poor water permeation barrier characteristics around 10^{-2} to 10^{-3} g m^{-2} per day.[8-12] In the organic/inorganic multilayer system, by interposing organic interlayers consisting of photo-curable polymers between adjacent inorganic films, the pathways for water vapor are considerably extended. In other words, defects between adjacent inorganic barrier films are

[a]POSTECH Organic Electronics Laboratory, Polymer Research Institute, Department of Chemical Engineering, Pohang University of Science and Technology, Pohang, 790-784, Republic of Korea. E-mail: cep@postech.ac.kr; sjoonseo@skku.edu
[b]SKKU Advanced Institute of Nanotechnology (SAINT) and Center for Human Interface Nanotechnology (HINT), Sungkyunkwan University, Suwon 440-746, Republic of Korea

decoupled by the organic interlayer. Therefore, water vapor needs more lag time to form a steady state flow across the barrier film. With this prolonged lag time, the barrier property of multilayer system is dramatically enhanced.[19,20] Together with the organic layer's own property, flexibility, the resulting organic/inorganic multilayer systems have unique characteristics in terms of not only passivation ability but also robustness against external stress.

Polymeric interlayer deposition processes toward multilayer passivation are generally performed under low-vacuum or atmospheric conditions *via* flash evaporation[21] or spraying methods that require additional equipment or experimental steps. Impurities arising from low-vacuum processes or residual additives from a monomer solution can potentially be incorporated into organic interlayers; hence, simple organic interlayer deposition methods under high-vacuum conditions are needed to decrease the time required for passivation during the preparation of high quality films and to increase production power.

Here, in this research, we used zinc diacrylate (ZDA) as a monomer for the organic interlayer of multilayer passivation. ZDA can be evaporated under high-vacuum conditions without deteriorating the polymer crosslinking properties. ZDA was deposited under high-vacuum conditions ($<10^{-5}$ Torr) and crosslinked under photoinitiator-free UV irradiation. The resulting polymeric zinc acrylate (pZA) film displayed successful conversion from a monomeric to a polymeric phase upon UV irradiation. The films displayed an increase in the breakdown voltage and photo-patternability as well as a high permeation activation energy of 53 kJ mol^{-1}. A multilayer passivation layer comprising 6.5 pairs of thermally evaporated pZA/silicon monoxide (SiO) layers was applied to flexible OTFTs. The passivated OTFTs displayed environmental stability with a prolonged lifetime compared to the non-passivated and SiO-only passivated devices, in addition to an enhanced robustness against physical stress with a nearly unchanged device performance after 500 bending experiments.

2. Experimental

ZDA film preparation and characterization

ZDA was purchased from Aldrich and used as received without further purification steps. ZDA was loaded into a thermal evaporator (SUNIC SUNICEL 0603) and evaporated at a rate of 0.5 Å s^{-1} under 10^{-5} Torr vacuum conditions. ZDA was easily evaporable in a conventional vacuum thermal evaporator without the need to modify the conventional system. The vacuum-deposited ZDA film was UV-exposed under a low-pressure Hg lamp (wavelength 254 nm) for 20 min in a nitrogen glove box to achieve sufficient photo-crosslinking among the acrylic monomers. The surface roughness of the ZDA before and after UV irradiation was studied by atomic force microscopy (AFM, VEECO Dimension 3100). The water vapor transmission rates (WVTRs) of pZA films were evaluated at 38 °C and 100% RH with a MOCON AQUATRAN-1. UV-vis transmittance and Fourier transform infrared spectroscopy (FTIR) measurements were conducted using JASCO V-600 and Nicoret 6700 instruments, respectively.

Flexible OTFT fabrication and passivation

A 50 nm thick Al layer was deposited onto a pre-cleaned poly-arylate (PAR) substrate with a thickness of 100 μm (AryLite™ A 100HC, Ferrania Technology) to form a gate electrode. Subsequently, an Al$_2$O$_3$ layer was over-coated to form a gate insulator with a thickness of 100 nm using a PEALD process. In the PEALD process, trimethyl aluminum (TMA) and oxygen (O$_2$) were used as the sources of Al and O, respectively. A 20 μs pulse plasma with a 100 W radio frequency power was applied during the PEALD process. The substrate temperature was fixed at 100 °C to ensure the stability of the PAR substrates during the PEALD deposition process. A 30 nm layer of cyclic olefin copolymer (Polyscience Co.) was spin-coated to provide a high-performance bilayer gate dielectric for preparing flexible OTFTs. The samples were then heated on a 120 °C hot plate for 30 min to remove any residual solvent. Subsequently, a 50 nm pentacene layer was patterned through a shadow mask by evaporation to form an organic semiconductor layer using an organic molecular beam deposition (OMBD) system. A 50 nm thick gold layer was applied to the pentacene using a vacuum thermal evaporator with 3 Å s^{-1} deposition rate and 10^{-5} Torr vacuum conditions to form the source/drain electrodes. The channel length (*L*) and width (*W*) of the shadow mask used for gold deposition were fixed at 100 μm and 1500 μm, respectively.[22] Multilayer passivation on flexible OTFTs was performed using silicon monoxide (SiO) as an inorganic counterpart of pZA. Layers of pZA (20 nm) and SiO (20 nm) were deposited onto the OTFTs in the same evaporation chamber (SUNIC SUNICEL 0603) by alternating evaporation cells under 10^{-5} Torr vacuum. 6.5 pairs of pZA/SiO stacks were applied to the flexible OTFTs to form a passivation layer. The configuration of the deposited multilayer was confirmed using HR-STEM (JEOL, JEM-2100F) and Focused Ion Beam (Helios, Pegasus) methods.

Device characterization

The electrical properties of the OTFTs were characterized using a home-built combination of Keithley 2400 and 236 source/measure units. The field effect mobilities (*μ*) of the OTFTs were calculated from the slope of the square-root of the drain current ($I_D^{1/2}$)/the gate voltage (V_G) plot. In the bending test, flexible OTFTs were exposed to a tensile stress under a 2.2 cm bending radius. The surface morphologies before and after the bending tests of the passivated OTFTs were characterized using an optical microscope (OM). The long-term stabilities of the OTFTs were tested by storing at 25 °C under a 60% RH conditioned environmental chamber. The electrical characteristics were measured over a time sequence.

3. Result and discussion

Before the polymerization steps for ZDA, the stable thermal evaporation of ZDA under heating was confirmed by performing an FTIR analysis of the thermally evaporated ZDA film on a Si wafer. As shown in Fig. 1(a), the peaks corresponding to the acrylate moiety at 1640 cm^{-1} (C=C stretching), 980 cm^{-1} (*trans* C–H and CH$_2$ out-of-plane deformation), and 830 cm^{-1} (CH$_2$ out of plane deformation) were observed in the deposited ZDA film after thermal evaporation. These absorption peaks are
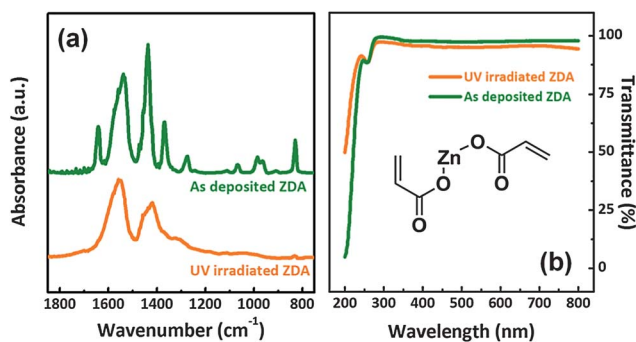
Fig. 1 (a) FTIR measurement data for as-deposited ZDA film with vacuum-thermal evaporation, and 20 min UV irradiated ZDA film. (b) UV transmittance spectra of a 200 nm ZDA layer on a quartz substrate: as-deposited ZDA sample, and the sample exposed to UV irradiation.

Fig. 2 (a) Optical microscopy (OM) images of photo-patterned pZA using UV irradiation through a photo mask. (b) Breakdown voltages of pristine ZDA and pZA. The inset shows a schematic image of the breakdown voltage measurement setup.

similar to the typical spectral peaks of ZDA.[23] This result indicated that the thermally evaporated ZDA films maintained their cross-linkable characteristics during heating for the thermal evaporation step.

ZDA monomers were polymerized by applying UV irradiation to the vacuum-thermally deposited ZDA films without the need for photoinitiators. Photoinitiators generally consist of low molecular weight materials, and their vapor pressure can be quite high; photoinitiators can, therefore, contaminate the chamber during thermal evaporation under high-vacuum conditions. Physical vapor deposition–polymerization steps require an excess amount of initiators compared to solution processes because the vapor-deposited films are immobile.[24] In view of these problems, there is a need to identify photoinitiator-free polymerization processes. Scherzer et al. reported that several types of diacrylate monomers can be polymerized without a photoinitiator upon exposure to photon energies on-resonance with the acrylate absorption peaks.[25] This novel polymerization process was implemented here by measuring the UV-vis transmittance spectrum of a ZDA film on a quartz substrate to determine the absorption peak. As shown in Fig. 1(b), a strong absorption band around 200 nm could be assigned to the polymerizable acrylate moiety. UV stimulation at the targeted wavelength was applied using a low-pressure mercury lamp (covering 30% of the 171 nm peak). After exposing the ZDA film to UV light for 20 min, the vinyl group-related peaks at 1640 cm^{-1}, 980 cm^{-1}, and 830 cm^{-1} were significantly reduced in the FTIR spectrum (Fig. 1(a)). The disappearance of the C=C stretching peak at 1640 cm^{-1} suggested that the double bond of the acrylate opened as a result of polymerization under UV irradiation. Slight shoulder peaks around 1300–1360 cm^{-1}, which were related to transversal and longitudinal deformations of the alkyl chain, also grew in as a result of the vinyl polymerization.[26] Interestingly, the UV-vis transmittance spectrum data shown in Fig. 1(b) suggested that both the vacuum-deposited and UV-exposed ZDA films on a quartz substrate displayed a high transmittance, exceeding 95% over the visible range (400–800 nm). A high transmittance in the visible range is useful for multi-purpose applications of ZDA layers in organic electronics, such as the passivation of transparent devices or top-emission OLEDs.

Fig. 2(a) shows optical microscopy (OM) images of ZDA films photo-patterned through a chrome patterned quartz mask. The
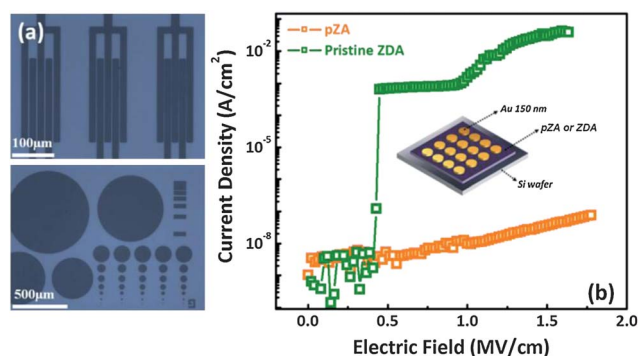
photo-pattern was obtained through 20 min UV irradiation of the as-deposited 100 nm ZDA film on a Si wafer through a photo mask, followed by dipping in isopropyl alcohol (IPA) for development. The resulting film, shown in Fig. 2(a), presented high-resolution patterns with a variety of shapes with channel spacings less than 10 μm.

The breakdown voltage was measured using the device configuration shown in the inset of Fig. 2(b). pZA and ZDA films were interposed between the heavily doped Si wafer and a 150 nm Au electrode. ZDA film showed about 8% thickness reduction (from 490 nm to 450 nm) because of polymerization and this effect was attributable to the field calculation for the accurate breakdown field measurement. A breakdown voltage exceeding 1.8 MV cm^{-1} was obtained, about 4 times larger than the value obtained for an as-deposited ZDA film (0.43 MV cm^{-1}). Generally, the increase in the breakdown voltage was related to an increase in the film density and a decrease in the number of voids in the film. We inferred from these results that UV exposure produced a condensed polymeric zinc acrylate film.[27,28]

Fig. 3 shows the atomic force microscopy (AFM) images of 100 nm thick as-deposited and pZA films on a Si wafer. The surface morphologies of the organic interlayers were considered to be critical for the barrier properties of the upper inorganic
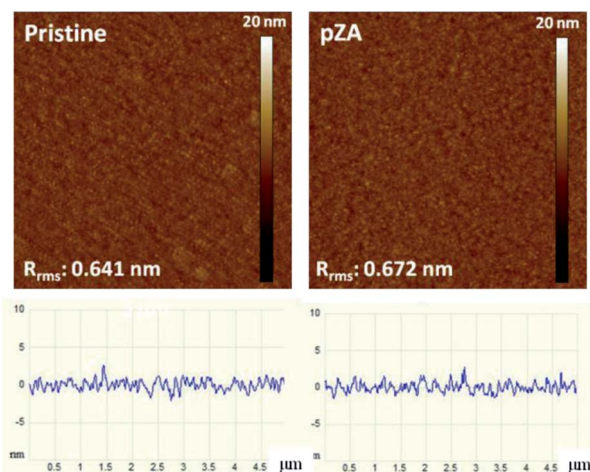
Fig. 3 AFM and cross-sectional images of the pristine and pZA films.
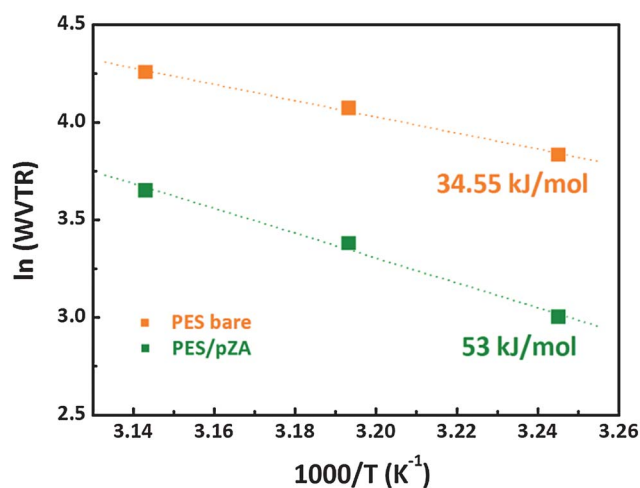
Fig. 4 Arrhenius plots of the permeability (P) as a function of temperature for the bare PES substrate and pZA 200 nm film on a PES substrate.

layer because surface abnormalities in the organic interlayer induced cracks or pinhole formation, which acted as permeation channels in the inorganic superstructure. The as-deposited ZDA films showed very smooth surfaces (R_{rms} 0.641 nm) without any noticeable particle formation, which could be introduced by spitting of the unstable source materials during deposition. In addition, we confirmed that the UV exposure used to cure the ZDA did not affect the surface morphology of the deposited film (R_{rms} 0.672 nm). The surface smoothness approached the value generally obtained for wet processed conventional polymeric interlayers.

The characteristics of the pZA film as a barrier were obtained by measuring the WVTR and the activation energy required for water vapor permeation. The WVTR of the 100 nm pZA on a 200 μm polyether sulfone (PES) substrate was 29.29 g m^{-2} per day, which resulted in approximately a two-fold barrier improvement factor (BIF) compared to the pristine PES film (58.59 g m^{-2} per day). The activation energy associated with permeation of a pZA film was determined by measuring the

WVTR at different temperatures and calculating the value according to the equation provided below,[29]

$$P = P_0 \exp\left(-\frac{E_a}{RT}\right)$$

where P is the permeability, P_0 is a constant system-dependent permeation coefficient, and E_a is the activation energy for permeation. The activation energy for permeation was determined from the linear slope of the fit to Fig. 4. Permeation activation energies of 53 kJ mol^{-1} and 34.55 kJ mol^{-1} were obtained for 100 nm pZA on PES and pristine PES films, respectively. The activation energy of permeation is the sum of all activation energies during the permeation of water vapor, including adhesion, solution, diffusion, and dissolution of the water molecules. Because the zinc acrylate polymer exhibited higher activation energy than conventional polymer films, such as PEN and PET, the pZA film may be resistant to the permeation of water vapor.[29]

The high activation energy for permeation, high transmittance, and processing advantages of ZDA as an organic interlayer were tested by applying multilayer passivation to flexible OTFTs. For the application of pZA interlayer for organic/inorganic multilayer passivation, thermally evaporated silicon monoxide (SiO) layer was adopted as an inorganic counterpart and applied onto flexible OTFT devices. The thermally evaporated SiO layer permitted all passivation processes to be performed in a single evaporation chamber by alternating between evaporation cells using cell shutters during the organic/inorganic multilayer deposition process. The use of a single chamber presented a tremendous improvement in terms of processing time, convenience and efficiency compared to conventional deposition processes.

A total of 6.5 pairs of pZA 20 nm/SiO 20 nm layers was applied to obtain multilayer passivation of a pentacene based dual gate dielectric OTFT on a polyarylate (PAR) substrate, and the barrier characteristics of this layer were evaluated. The transfer and output characteristics of flexible OTFTs are shown in Fig. 5(a) and (b), respectively. The field effect mobilities (μ) of OTFTs were obtained from the slope of a plot of the square root
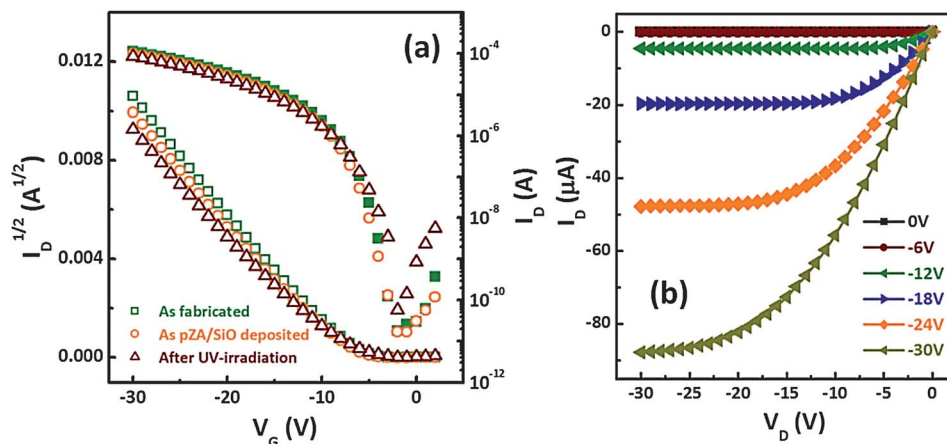
Fig. 5 (a) Transfer characteristics of as-fabricated, ZDA/SiO 6.5 pair deposited and UV-induced polymerized 6.5 pair ZDA/SiO deposited OTFTs. (b) Output characteristics of as-fabricated flexible OTFTs.

of drain current (I_D) *versus* the gate voltage (V_G) in the saturation current region using the equation below;[3]

$$I_D = \left(\frac{WC_i}{2L}\right)\mu(V_G - V_{th})^2$$

where I_D is the drain current, C_i is the capacitance per unit area of the dielectric. W and L are the channel width and length, respectively. As fabricated flexible OTFT devices exhibit a mobility of 0.73 ± 0.06 cm^2 V^{-1} s^{-1}. In addition, as shown in Fig. 5(b), the OTFTs showed good linear/saturation characteristics with the operating voltage range of -30 V and apparent leakage current was not observed at zero drain voltage. During the passivation process, the mobility of passivated OTFTs is slightly degraded to 0.63 ± 0.06 cm^2 V^{-1} s^{-1} (Fig. 5(a)). The slight reduction of mobility is probably due to the UV irradiation during the passivation process. However, the performance degradation is not severe because the UV transmittance of 6.5 pairs ZDA/SiO multistack around 250 nm, which is the main wavelength of a low pressure mercury lamp, was less than 5% (not shown here).

The inset of Fig. 6(c) shows images of bent OTFTs covered with a passivation layer, and Fig. 6(a) shows a TEM cross-sectional image of 6.5 pairs of pZA/SiO layers on a Si wafer prepared during the batch OTFT passivation step. Cross-sections were obtained using focused ion beam (FIB) cutting. As shown in the energy-dispersive spectral (EDS) images in Fig. 6(b), atomic zinc (red) and silicon (green) were detected in the cross-sectional profiles. The flexibility of the pZA/SiO multilayer was tested by submitting the passivated flexible OTFT devices to 500 repetitions of bending stress (to a radius of 2.2 cm). Fig. 6(d) and (e) show optical microscopy images of OTFT channel regions passivated with SiO 120 nm or 6.5 pairs of pZA/SiO layers, respectively, and exposed to bending stress. For the OTFT passivated with SiO-only, 10 bending repetitions were sufficient to induce severe damage in the channel region, seriously deteriorating the output characteristics of the device [the mobility and on–off ratio decreased from 0.67 cm^2 V^{-1} s^{-1} and 1.41×10^6 to 0.32 cm^2 V^{-1} s^{-1} and 1.8×10^4, respectively, see Fig. 6(c)]. This degradation was attributed to damage of the

source/drain electrodes and the channel regions of the OTFTs due to cracking of the SiO upper barrier film. By contrast, 7 layers of pZA incorporated into the OTFTs between the 120 nm SiO layers displayed constant device characteristics, even after 500 bending repetitions. No cracks were observed in the channel regions of the devices (Fig. 6(e)).

The stability of the pZA/SiO multilayer passivated OTFT was investigated by time-dependent electrical performance measurements in a chamber with constant environmental conditions: 25 °C, 60% RH and dark. 500 times bent (bending radius 2.2 cm) OTFTS with pZA/SiO passivation film was also stored in the environmental chamber in order to confirm the stability of the pZA/SiO barrier film against bending stress.

Fig. 7 shows the time-dependent $I_D^{1/2}$ *versus* V_G (gate voltage) characteristics of the flexible OTFTs. As shown in Fig. 7(a), non-passivated devices showed a dramatic reduction in current after 97 days of measurement. A similar trend was observed in devices passivated with only a 120 nm SiO layer (Fig. 7(b)). By contrast, devices passivated with 6.5 pairs of pZA/SiO layers showed similar transfer characteristics in the as-fabricated samples and the samples stored for 97 days in the environmental chamber (Fig. 7(c)). In addition, the sample that had been bent 500 times showed almost unchanged transfer characteristics after 97 days of storage (Fig. 7(d)). Similar trends were observed in the time-dependent mobility variations in the OTFTs, Fig. 8. The OTFTs prepared without a passivation layer and passivated with only SiO 120 nm showed a dramatic degradation in μ after 97 days of storage. Both OTFTs showed a mobility that was less than 6% of the value for the fresh devices (a decrease from 0.73 ± 0.06 to 0.036 ± 0.01 cm^2 V^{-1} s^{-1} for bare OTFTs and from 0.69 ± 0.04 to 0.035 ± 0.04 cm^2 V^{-1} s^{-1} for SiO 120 nm only OTFTs). By contrast, the pZA/SiO multilayer-passivated devices and the samples bent 500 times exhibited mobilities after 97 days of storage that were comparable to the initial mobilities of 0.63 ± 0.03 cm^2 V^{-1} s^{-1} and 0.67 ± 0.03 cm^2 V^{-1} s^{-1}, respectively, and final mobilities of 0.58 ± 0.02 cm^2 V^{-1} s^{-1} and 0.62 ± 0.03 cm^2 V^{-1} s^{-1}, respectively. These results suggest that the incorporation of a pZA interlayer into the inorganic barrier films enhanced the permeation barrier characteristics.
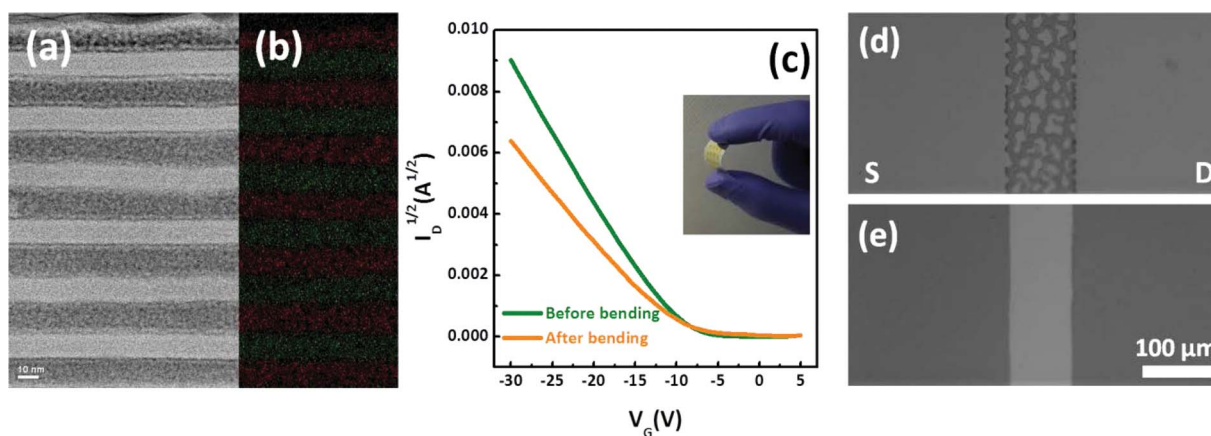
Fig. 6 (a) TEM cross-sectional images of 6.5 pairs of a pZA/SiO multilayer film. (b) Atomic mapping image of the multilayer film using TEM-EDS (red: Zn, green: Si). (c) Electrical characteristics of flexible OTFTs passivated with a 120 nm SiO layer before and after bending (inset: bending image of flexible OTFTs with 6.5 pairs of pZA/SiO multilayer passivation). Optical microscopy images of the channel regions of (d) a 120 nm SiO layer and (e) 6.5 pairs of pZA/SiO layers after bending.
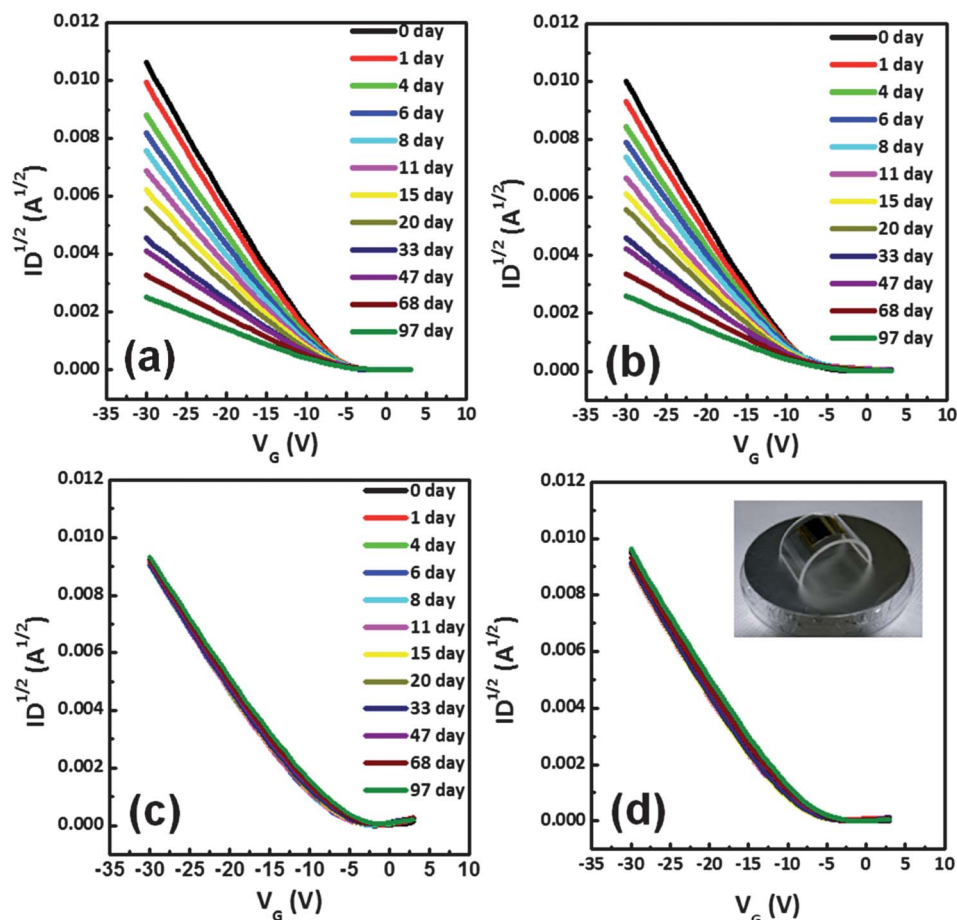
Fig. 7 Time-dependent $I_D^{1/2}$ versus V_G characteristics of (a) bare OTFTs, (b) a 120 nm SiO passivated OTFT, (c) a passivated OTFT formed from 6.5 pairs of pZA 20 nm/SiO 20 nm layers, and (d) 500 repetitions of OTFT bending (inset: image of an OTFT bent over a 2.2 cm radius) after application of 6.5 pZA/SiO pairs for passivation. All electrical measurements were performed under 25 °C, 60% RH environmental chamber conditions.
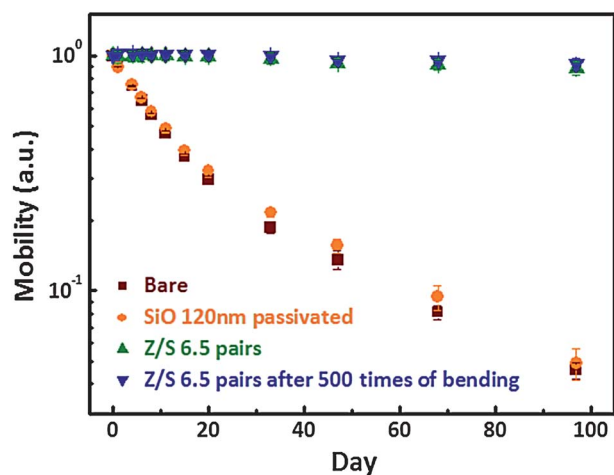
Fig. 8 Time-dependent field-effect mobilities of bare, 120 nm SiO-passivated, 6.5 pZA/SiO pair-passivated, and 6.5 pZA/SiO pair-passivated flexible OTFTs submitted to 500 bending repetitions (25 °C, 60% RH environmental chamber conditions).

The above-mentioned lifetime enhancement in the passivated OTFTs could be related to the barrier property enhancement by quantifying the water vapor permeation by measuring the WVTR

Table 1 WVTR data for pZA 20 nm/SiO 20 nm multilayer passivation with various numbers of layer pairs

	PEN bare	pZA 140 nm	SiO 120 nm	pZA/SiO 2.5 pairs	pZA/SiO 4.5 pairs	pZA/SiO 6.5 pairs
WVTR (g m^{-2} per day)	1.324	1.231	1.207	0.643	0.19	0.055

values of the passivation layers. A 200 μm polyethylene naphthalate film (PEN) was used as a substrate for testing the pair variation. As shown in Table 1, an increase in the pairs was associated with a decrease in the WVTR values of the multilayer films, corresponding to a dramatic enhancement in the barrier properties. The presence of 6.5 pairs of pZA layers in the 120 nm SiO film yielded a 25-fold barrier enhancement compared to a single 120 nm SiO film (0.055 g m^{-2} per day for the pZA/SiO multilayer, 1.207 g m^{-2} per day for the 120 nm SiO layer). These trends were similar to the OTFT electrical property degradation characteristics. The device data and MOCON results indicated that pZA performed well as an interlayer in a multilayer barrier system. Compared to the conventional flexible multilayer systems using plasma based deposition methods (PECVD, PEALD),[30,31] WVTR (0.055 g m^{-2} per day) of 6.5 pairs pZA/SiO multilayer

passivation shows a higher value. This result is closely related to poor barrier characteristics (1.207 g m^{-2} per day) of vacuum thermally evaporated SiO which played a role as a main barrier film in the multilayer system. Nevertheless, even with poor barrier films such as SiO, pZA improved the barrier characteristics and supported the device characteristics of the OTFTs during 97 days of storage under environmental chamber conditions.

4. Conclusion

In summary, vacuum-thermally evaporated ZDA was used as a monomer to prepare a polymeric interlayer for inorganic/organic multilayer passivation. The vacuum-thermally evaporated film showed the successful conversion to a polymeric phase under direct UV irradiation without the need for photoinitiators. The resulting film showed a smooth surface, was photopatternable, and exhibited a large breakdown field and large activation energy for water permeation. In a real device application, a flexible OTFT passivated with a pZA/SiO multilayer showed a prolonged lifetime exceeding 97 days. Even with 500 bending repetitions (with a radius of 2.2 cm), the pZA/SiO multilayer retained its barrier properties and showed degradation characteristics similar to those of non-bent devices. In addition, the MOCON results indicated a 25-fold barrier enhancement for the 6.5 paired pZA/SiO layer barrier relative to the 120 nm SiO-only deposited devices.

Acknowledgements

References

1 T. W. Kelley, P. F. Baude, C. Gerlach, D. E. Ender, D. Muyres, M. A. Haase, D. E. Vogel and S. D. Theiss, *Chem. Mater.*, 2004, **16**, 4413.
2 D. Li, E.-J. Borkent, R. Nortrup, H. Moon, H. Katz and Z. Bao, *Appl. Phys. Lett.*, 2005, **86**, 042105.
3 Y. Wen, Y. Liu, C. Di, Y. Wang, X. Sun, Y. Guo, J. Zheng, W. Wu, S. Ye and G. Yu, *Adv. Mater.*, 2009, **21**, 1631.
4 K. Lee, J. Y. Kim, S. H. Park, S. H. Kim, S. Cho and A. J. Heeger, *Adv. Mater.*, 2007, **19**, 2445.
5 C. Charton, N. Schiller, M. Fahland, A. Holländer, A. Wedel and K. Noller, *Thin Solid Films*, 2006, **502**, 99.
6 M. Schaer, F. Nüesch, D. Berner, W. Leo and L. Zuppiroli, *Adv. Funct. Mater.*, 2001, **11**, 116.
7 S. J. Lewis and S. M. Weaver, *IEEE J. Sel. Top. Quantum Electron.*, 2004, **10**, 45.
8 H. K. Kim, M. S. Kim, J. W. Kang, J. J. Kim and M. S. Yi, *Appl. Phys. Lett.*, 2007, **90**, 013502.
9 H. Jeon, K. Shin, C. Yang, C. E. Park and S. H. Park, *Appl. Phys. Lett.*, 2008, **93**, 163304.
10 J. Meyer, P. Gorrn, F. Bertram, S. Hamwi, T. Winkler, H. Johannes, T. Weimann, P. Hinze, T. Riedl and W. Kowalsky, *Adv. Mater.*, 2009, **21**, 1845.
11 A. Dameron, S. Davidson, B. Burton, P. Carcia, R. McLean and S. M. George, *J. Phys. Chem. C*, 2008, **112**, 4573.
12 A. Sugimoto, H. Ochi, S. Fujimura, A. Yoshida, T. Miyadera and M. Tsuchida, *IEEE J. Sel. Top. Quantum Electron.*, 2004, **10**, 107.
13 S. Nam, H. Jeon, S. H. Kim, J. Jang, C. Yang and C. E. Park, *Org. Electron.*, 2009, **10**, 67.
14 S. Nam, J. Jang, K. Kim, W. M. Yun, D. S. Chung, J. Hwang, O. K. Kwon, T. Chang and C. E. Park, *J. Mater. Chem.*, 2011, **21**, 775.
15 S. Cho, K. Lee and A. J. Heeger, *Adv. Mater.*, 2009, **21**, 1941.
16 P. Burrows, G. Graff, M. Gross, P. Martin, M. Hall, E. Mast, C. C. Bonham, W. D. Bennett, L. A. Michalski, M. S. Weaver, J. J. Brown, D. Fogarty and L. S. Sapochak, *Proc. SPIE–Int. Soc. Opt. Eng.*, 2001, **4105**, 75.
17 A. Dameron, S. Davidson, B. Burton, P. Carcia, R. McLean and S. M. George, *J. Phys. Chem. C*, 2008, **112**, 4573.
18 Y. C. Han, C. Jang, K. J. Kim, K. C. Choi, K. H. Jung and B. S. Bae, *Org. Electron.*, 2011, **12**, 609.
19 G. L. Graff, R. E. Williford and P. E. Burrows, *J. Appl. Phys.*, 2004, **96**, 1840.
20 J. Greener, K. C. Ng, K. M. Vaeth and T. M. Smith, *J. Appl. Polym. Sci.*, 2007, **106**, 3534.
21 P. E. Burrows, G. L. Graff, M. E. Gross, P. M. Martin, M. K. Shi, M. Hall, E. Mast, C. Bonham, W. Bennet and M. B. Sullivan, *Displays*, 2001, **22**, 65.
22 J. Jang, S. Nam, D. S. Chung, S. H. Kim, W. M. Yun and C. E. Park, *Adv. Mater.*, 2010, **20**, 2611.
23 Aldrich Chem. Co, *The Aldrich Library of FT-IR Spectra*, Aldrich, Milwaukee, 1997, vol. 1, p. 872.
24 M. Muroyama, S. Yokokura, K. Tanaka and H. Usui, *Jpn. J. Appl. Phys.*, 2010, **49**, 01AE03.
25 T. Scherzer, *J. Polym. Sci., Part A: Polym. Chem.*, 2004, **42**, 894.
26 K. Senda, S. Sotowa, K. Tanaka and H. Usui, *Surf. Coat. Technol.*, 2011, **206**, 884.
27 D. D. Burkey and K. K. Gleason, *J. Appl. Phys.*, 2003, **93**, 5143.
28 J. Jang, S. H. Kim, J. Hwang, S. Nam, C. Yang, D. S. Chung and C. E. Park, *Appl. Phys. Lett.*, 2009, **95**, 073302.
29 B. M. Henry, A. G. Erlat, A. McGuigan, C. R. M. Grovenor, G. A. D. Briggs, Y. Tsukahara, T. Miyamoto, N. Noguchi and T. Niijima, *Thin Solid Films*, 2001, **382**, 194.
30 H. K. Kim and C. K. Cho, *Nanoscale Res. Lett.*, 2012, **7**, 69.
31 T. S. Kwon, D. Y. Moon, Y. K. Moon, W. S. Kim and J. Y. Park, *J. Nanosci. Nanotechnol.*, 2012, **12**, 3696.

This journal is © The Royal Society of Chemistry 2012

J. Mater. Chem., 2012, **22**, 25395–25401 | 25401